Catalogue of Young Stellar Objects

Attila Moór, Péter Ábrahám, Ágnes Kóspál, Attila Juhász, Csaba Kiss

2006

Contents

1 Introduction

Young stellar objects (YSOs), due to their dusty environment, are popular targets of infrared space telescopes. The Infrared Space Observatory (ISO) played a significant role in collecting new observational data needed to understand better the different stages of star formation. In our new photometric catalogue we collect and reprocess a sample of ISOPHOT observations (measured in the framework of different observing programmes), whose targets were young stellar objects. This catalogue differs from our previous ones, because it contains observations from several observing modes (e.g. mini-map, staring and scan mode), while our previous HPDP products always focused on one specific observing mode at a time.

2 Sample selection

We made a systematic search in the ISO Data Archive (IDA) for ISOPHOT photometric observations of young stellar objects. The query focused on compact objects (smaller or comparable to the beam), and excluded nebulous extended sources. Spectrophotometric measurements obtained with the ISOPHOT-S subinstrument, as well as large maps of star forming regions will be presented in separate HPDP catalogues. From the far-infrared C100/C200 observations we selected only those whose observing mode has already been re-calibrated as part of our previous HPDP projects (Moór et al. 2003, 2005). Thus e.g. chopped observations with the C100 detector were discarded because this submode has not been re-calibrated yet.

The statistics of the selected observations, separated per observing programmes is listed in Table 1. Most programmes intended to produce spectral energy distributions of YSOs, but there were a few dedicated projects on long term monitoring of young stars, too. These monitoring programmes we evaluated in a non-standard way in order to increase the relative photometric accuracy within the "IR light curve" (for details see Sect. 4).

3 Brief description of the utilized observing modes

ISOPHOT consisted of three detector subsystems or subinstruments (PHT-P, PHT-C, PHT-S). Each of them was optimised for specific photometric modes and only one could be used at a time. Observations included in this catalogue were performed using the PHT-P and PHT-C subsystems in various observing modes. In the following we very briefly described the main modes; for more detailed descriptions we refer to the ISOPHOT Handbook, as well as our previous HPDP reports (Moór et al. 2003, 2005).

3.1 Observations with the PHT-P detector subsystem

PHT-P was a multi-aperture photometer with three single element detectors (P1,P2,P3). 14 different filters and 12 apertures ranging from 5″to 180″were available to measure the infrared spectral distribution in the wavelength range from 3 to 120 μm.

Selecting the PHT03 astronomical observing template (AOT) one could perform photometric observations in one or more filters, either in staring or chopping mode, with the PHT-P subinstrument. In the ON-OFF mode separate staring observations were performed at the source and 1 background position. In a few cases more than one background position were observed either in a form of small incomplete maps or 3-point scans across the source, which was repeated several times (nodding observations). Another possibility to obtain ON-OFF measurements was to use the chopping mirror in the focal plane which regularly alternated in the beam between the source and the background position without moving the satellite.

Proposal ID	Observer	Observing modes	No. of related TDTs in the catalogue
1YSOSEDB	SVWB	PHT03 nodding, scan	7
2YSOSED	SVWB	PHT22 scan, mini-map	4
BINTTAU	CLEINERT	PHT22 scan, PHT37-39 sparse map	21
BIN_ADD1	CLEINERT	PHT22 scan, mini-map	8
CAS_CEP	TPRUSTI	PHT22 scan	6
CLASS0	JEISLOEF	PHT22 scan, mini-map	12
COLDDU_1	LHAIKALA	PHT22 scan	1
COLDDU_2	LHAIKALA	PHT22 scan	1
DEBRIS17	EBECKLIN	PHT22 mini-map	2
DEBRIS31	EBECKLIN	PHT22 mini-map	13
DEBRIS32	EBECKLIN	PHT22 mini-map	8
DISK_W01	HZINNECK	PHT22 mini-map	12
DOBASHI1	KDOBASHI	PHT22 mini-map	2
EXORS	GSTRINGF	PHT22 mini-map	7
FUOREXLU	TPRUSTI	PHT03 mapping, on-off, PHT22 scans	17
GUEST_01	RGUESTEN	PHT22 map	15
HERBIG2	CLEINERT	PHT03 scan, PHT22 mini-map	2
HERBIGAE	CLEINERT	PHT22 scan, chopped observation, PHT37-39 sparse map PHT03 on-off observation, mapping, chopping PHT17,19 sparse map	9
HERBSCAN	PABRAHAM	PHT22 scan	1
PROST0	RCHINI	PHT22 mini-map	5
PROSTATA	RCHINI	PHT22 mini-map	1
SBDSK1_A	SVWB	PHT37-39 sparse map	15
SBDSK2_A	SVWB	PHT37-39 sparse map	14
SF_CAS01	TPRUSTI	PHT22 mini-map	3
SF_CAS02	TPRUSTI	PHT22 mini-map	5
SF_CHA01	TPRUSTI	PHT22 mini-map	1
SF_TAU01	TPRUSTI	PHT22 mini-map	1
SF_TAU02	TPRUSTI	PHT22 mini-map	2
SF_TAU03	TPRUSTI	PHT22 mini-map	5
SURVEY_3	LNORDH	PHT37-39 sparse map	21
SURVEY_4	LNORDH	PHT22 scan, mini-map, PHT37-39 sparse map	15
VARIABL2	TPRUSTI	PHT03 on-off	2
VARIABL6	TPRUSTI	PHT03 on-off	2
VARIABL7	TPRUSTI	PHT03 on-off	2
VARIABLE	TPRUSTI	PHT03 on-off	24
VARICONT	TPRUSTI	PHT03 on-off	9
VARISED1	TPRUSTI	PHT22 mini-map PHT03 on-off	13

Table 1: *Main characteristics of the selected data sets*

3.2 Observations with the PHT-C detector subsystem

The PHT-C subsystem was composed of two far-infrared detector arrays: (1) C100 was a 3×3 array operating with 6 filters between 45 and 130 μm, (2) C200 consisted of 4 detector pixels (2×2 array) and could be used with 5 different filters between 90 and 240 μm. The projected pixel sizes on the sky were $43\farcs5\times43\farcs5$ for C100 and $89\farcs4\times89\farcs4$ for C200. In the case of PHT-C observations the field of view was defined by the area of the detector arrays (no aperture selection is required).

The PHT22 AOT performed photometry using specific filters belonged to the PHT-C subinstrument. This AOT could be used in the chopping and staring mode as well. **PHT22 scans** were one-dimensional rasters of 3 or more points with the source at the centre position. The **mini-map mode** was one of the most efficient ways of obtaining point source photometry with the C100 and C200 detectors. It was also the mode used for FCS calibration observations. C100 mini-maps are typically 3×3 raster maps performed in satellite coordinate system centered on the source. In the recommended and most frequently used configuration odd number of raster steps were performed with raster step size of 46″in both directions. For the C200 detector in the usual configuration the raster step size was 92″in combination with even number of raster steps in both direction.

Sparse map observations were executed in the concatenated sequence of PHT37, PHT38,

PHT39 Astronomical Observation Templates. Sparse map AOTs were designed to measure a sequence of irregularly spaced positions within an area of 3 degrees in diameter, with the first selected position determining the centre. Typical targets were a cluster of sources in a small area. It is worth mentioning that the detector remained switched-on all the time so the signal stability was increased and the times for overheads were reduced.

4 Data reduction

In the following we describe our data reduction, which was applied for most of the sources. The only exception was the data set on Herbig Ae/Be stars published by Ábrahám et al. (2000), in which case we adopted published flux values (PROPID: HERBIG2, HERBIGAE, HERBSCAN).

Our standard processing scheme can be separated into two main levels. At the first processing level we used the **P**HOT **I**nteractive **A**nalysis (PIA) version 10.0 Gabriel et al. (1997) software combining with separated IDL codes to reduce observations from the lowest data level (Edited Raw Data, ERD) to the final AAP (Auto Analysis Product Data) level. Correction for instrumental effects (e.g. the glitches induced by cosmic particles) as well as flux calibration was performed in this processing phase (see Sect. 4.1 for more details). At the second level, flux of the target object was extracted from the AAP data stream and then empirical corrections were applied.

4.1 Processing from raw data to AAP level

Table 2 outlines processing steps at the subsequent PIA data levels. Our scheme contains two corrections in addition to the general PIA processing steps. Both the dynamic transient correction and the drift correction were performed at the SRD level.

The dynamic transient correction has been developed in a joint project of the ISOPHOT Data Centre at MPIA and the Konkoly Observatory. This method fits the temporal signal evolution within a measurement by interpolating within a library of signal dependent transient curves and predicts the signal at t = 128s (for details see del Burgo et al., 2003). The transient correction was applied following the reset interval correction at the SRD level.

A mini-map or a longer scan measurement lasts a few hundred seconds, and on this timescale slow baseline variations, called 'long term drift' may not be negligible. The drift is usually positive, i.e. the signal increases with time even in the case of constant illumination. In order to correct for artifacts related to this effect we performed a 2nd order polynomial fit to the off-source raster step signals per pixel (as the function of time), and corrected the measurement according to the fit (for details see Moór et al., 2003).

The ISOPHOT instrument hosts two Fine Calibration Sources (FCSs) which were used as photometric standards to monitor the time evolution of the PHT-P and PHT-C detector responsivities. The two devices were identical and could be operated independently. Each ISOPHOT AOT (except PHT40) contained at least one FCS measurement which could be used to calculate the actual responsivity of the given detector. If an FCS measurement proves to be inadequate to determine the detector responsivity, the default responsivity could be used[1].

Since in most observing modes each observation is bracketed by two FCS measurements, there are several possibilities how to combine the two responsivity values. In the case of PHT22 scan and mini-map observations we used the averaging method to calculate the responsivities (it is the default method in PIA V10.0). For measurements in a longer sparse map sequence, responsivities were calculated from an interpolation between the two FCS measurements.

In those cases (PHT03 ON-OFF, chopping observations) where we had only one FCS measurement we used the actual responsivity value.

[1]The default responsivity is a function of the orbital phase and originally was determined by averaging many responsivity measurements from the whole mission (assumed that it does not vary from revolution to revolution).

PIA data levels	Applied calibration and processing steps	Notes for different observing modes
ERD (Edited Raw Data) to SRD (Signal per Ramp Data)	Ramp Linearization Ramp Deglitching (2threshold method)	
SRD to SCP (Signal per Chopper Plateau Data)	Reset Interval Correction **Dynamic Transient Correction** Dark Current Subtraction (orbit dependent) Signal Linearization Signal Deglitching **Drift correction** Combine signals	only for C100 data only for C100 and C200 scans and mini-maps
SCP to AAP (Auto Analysis Product Data)	Calculate FCS responsivities Convert signals to monochromatic flux densities per pixel per raster position	

Table 2: *Applied calibration and processing steps at different processing levels of PIA V10. Processing steps where separated IDL codes were used are typed in bold face.*

4.2 Flux extraction and empirical correction

4.2.1 PHT22 observations

In order to achieve good accuracies for point source photometry we used PSF fitting to extract fluxes from AAP data streams. Since the PSF is not well sampled in PHT22 observations and the ISO pointing was good to within $2''$, in most cases we assumed that the source is at the centre of the raster (the relevant observing modes were designed to measure the flux density of a source, which locates at the centre of the raster). We differed from this scheme in the following cases:

1. when same objects were measured several times – sometimes in different observing modes – and the central position of the target differs from each other. In order to keep a uniform position for the different observations we used the SIMBAD coordinates of the object in these cases.

2. if it was emerged, that this assumption is not correct, either because (a) the SIMBAD position of the original target differs from the position of the raster's centre by more than $10''$; (b) the final AAP map revealed that the position of the observed IR source differed from the central position; (c) the final AAP map showed additional sources in the observed region.

In 2 a-c cases we searched the Spitzer Science Center (SSC) data archive for Spitzer MIPS (Multiband Imaging Photometer for Spitzer) images of the same region. For those observations where higher spatial resolution infrared maps obtained by MIPS instrument at 24 or 70μm are available, we used the pipeline data (2-dimensional FITS image files) to check the position of the questionable object or objects. In the lack of MIPS images we estimated the coordinates on the basis of ISOPHOT maps. In some cases this position coincided well with the position of a nearby SIMBAD object (not the original target), offering a good opportunity to replace our coarse coordinates by more accurate ones.

Whenever it was possible (if a bright source measured in the C100 mini-map mode) we checked whether the source is extended. In the course of flux extraction and check for point/extended nature of the object we used the new measured beam profile - developed in the framework of a collaboration between the Konkoly Observatory and the ISOPHOT Data Centre

For mini-maps our flux extraction method is based on the determination of fluxes from the data stream of each individual pixel. In a usual mini-map with the source located at the centre of the raster each detector pixel observed the source, producing nine or four independent flux

density values in the case of C100 or C200 observations, respectively. The final source flux was derived from the average of these values. In the case of C100, after extensive systematic tests, we chose a robust averaging method called "bi-weight mean", while in the case of C200 observations the combination of the individual flux densities of the four detector pixels was performed by simple average. Uncertainties were computed from the dispersion of the individual results. After flux extraction we applied an empirical correction for all measurements. This correction is of additive nature at low flux level and of multiplicative nature at high flux level (for details see Moór et al., 2003).

Unlike in mini-map mode in C100 scan measurements not every detector pixel observes the source (in several C100 scan observations only pixel #5 was illuminated by the source at the centre of the raster) and the number of background positions may also be limited. In scan observations with C200 camera generally the source was placed on the centre of the array. Thus all four pixels detected the source, but only at the pixel corner resulting in decreased signal to noise. For C100 observations, where at least two pixels saw the source (for instance: scan measurements with raster step size of 46", where pixel #2, #5 and #8 saw the source) and for C200 observations we used similar method to extract source flux from the AAP data as in the case of mini-map observations. For those C100 scan maps, where the source illuminated only one pixel, we used a different extraction scheme. As a first step a flat-field array was calculated - using measurements on background raster positions - by normalizing fluxes to the pixel illuminated by the source. After flat-field correction was applied, the source flux can be extracted from the data stream of the second raster position using our PSF fitting method. As a last step we applied our empirical correction process for all scan measurements (for details see Moór et al. 2005).

4.2.2 PHT37-39 observations

Sparse map observations included in this catalogue were obtained by the C100 detector array. A typical sparse map sequence was composed of several staring measurements obtained at different background and source positions. Since in most cases point sources were positioned at the centre of the C100 camera (targets were observed by pixel #5 only), we used the "flat-field method" in the course of flux extraction. For a specific source measurement the flat-field array was determined using an interpolation between the flat-field values computed from individual background measurements along the sequence. After flat-field correction was applied, the source flux can be extracted from the data stream of the source measurements using the measured beam profile. It should be noted that the first measurements in a sequence turned out to be less reliable due to the non-stabilized signal (they are marked by a specific quality flag in the catalogue).

4.2.3 PHT03 observations

In PHT03 observations the source flux was determined by subtracting the flux measured towards the background position from the on-target measurement (ON/OFF,chopping). When several background positions were available they were averaged before subtraction (mapping, nodding).

4.2.4 Monitoring programmes

A subsample of ISOPHOT YSO observations was devoted to study the mid- and far-infrared variability characteristics of young stars. In these type of programmes the accuracy of absolute calibration is less important, since they focus on the variations of flux. We developed a new method for relative flux calibration of monitoring observations.

In a typical monitoring programme usually similar observing strategy was adopted at each epoch. It means that the measurement setup - especially the FCS heating power and the filter sequence - was identical for a number of epochs. This similarity of the observing sequences helps to handle the detector transients and achieve better accuracies. Even though the detector signals did not stabilize in most cases, because of the identical observing strategy and flux history the

shape of the transient curves were similar on all days. The first step of our new processing method is to compare the SRD curves of FCS measurements obtained at two different epochs in a very different way, by dividing the two FCS curves on a signal-by-signal basis and computing an average scaling factor between them. Then the obtained scaling factor is applied on the sky measurements as well, in order to correct for responsivity differences on the two days. The ratio of the scaled sky signals reflects true brightness difference between the two days. Figure 1 shows the result of the signal scaling in the case of observations of SV Cep (using P3 detector at 100μm). In the final step the absolute brightness can be calculated by multiplicating the

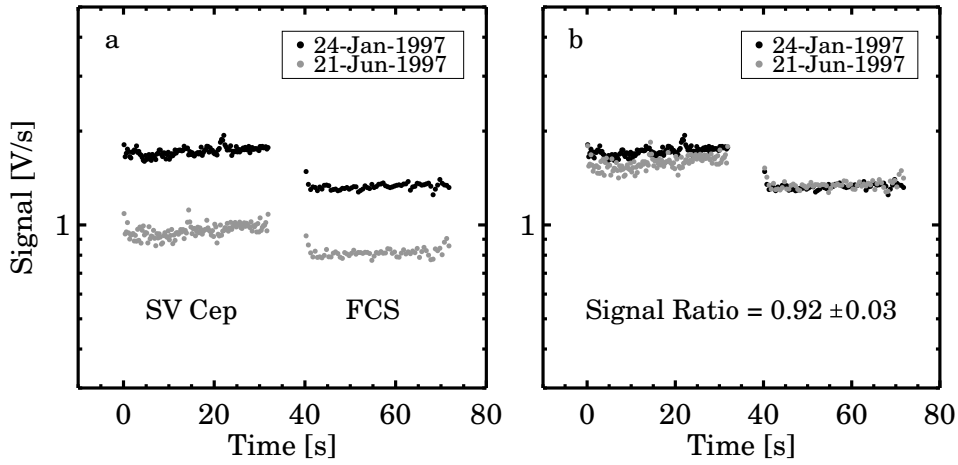

Figure 1: *Scaling of the signals in the case of 100μm measurements.*

normalized curve with the calibrated flux value of the reference day (here one can adopt e.g. the OLP10 calibration). This new method gives the flux ratio of the target at two different epochs with high accuracy (better than 10%.). For more details related to the data reduction of monitoring observation see Juhász et al. (2006).

5 Individual cases

5.1 Additional sources on maps

To be compatible with the present structure of the ISO Data Archive, in those cases where more than one source can be found on a map, the catalogue and the assigned postcard and survey product only shows the basic parameters of that target which is closest to the centre of the map (usually this was the intended target of the observer). The data of additional sources, which are not included in the catalogue, are summarized in Table 3.

The presence of [TMM99b] MMS 2, NAME LDN 1455 smm 1, NAME IC 348 MMS on the ISOPHOT maps was originally revealed by Froebrich et al. (2003).

5.2 Special sparse maps

In a typical sparse map sequence point sources were positioned at the centre of the C100 or C200 camera, and these "ON" measurements were spatially separated so the arrays did not overlap on the sky. However, in some sparse map sequence targets were very close to each other and therefore the arrays overlapped on the sky. This means that a specific source were observed at different array positions and on the other hand arrays at a specific position could contain more than one source. In order to extract fluxes from such situations we combined information from the different sparse map steps using the measured beam profile placed at the known positions of the YSOs.

In order to keep the compatibility with the IDA – although several measurements were used to derive the flux density for a specific source – in these cases we linked only that sparse map

TDT number	Original source	Additional source or sources	Wavelength [μm]	Flux density [Jy]	Flux uncertainty [Jy]
56300710	[TMM99b] MMS 4	[TMM99b] MMS 2	170	79.5	21.1
			200	51.5	5.3
65903004	NAME RNO 15 FIR	NAME LDN 1455 smm 1	170	10.2	4.6
			200	22.5	4.8
65903102	NAME HH 211 FIR	NAME IC 348 MMS	170	44.2	6.2
			200	35.4	11.7
69802504	[AVE98] HH 24-26 3	[AVE98] HH 24-26 4	120	45.3	4.1
			200	101.6	7.1
		2MASS J05460722-0013231	120	92.8	8.3
			200	147.7	21.5
84402015	NAME LDN 1448 IRS 3	LDN 1448C	200	116.2	8.1
56300709	[TMM99b] MMS 4	[TMM99b] MMS 2	60	5.4	0.8
			100	30.4	6.0
65903003	NAME RNO 15 FIR	NAME LDN 1455 smm 1	60	5.2	0.9
			100	9.3	3.2
65903101	NAME HH 211 FIR	NAME IC 348 MMS	60	1.56	0.66
			100	1.5	1.15
27101206	[CCE98] 1- 40	NAME CED 111 IRS 4	80	8.4	0.6
		[CCE98] 1- 42	80	5.6	0.9
26101506	[CCE98] 1- 40	[CCE98] 1- 42	150	45.1	18.8
80001905	LkHa 198	V376 Cas	4.8	10.6	2.6
			7.7	16.1	4.0
			10.0	19.6	4.9
78201506	LkHa 198	V376 Cas	12.8	22.9	5.7
			15.0	28.1	7.0
78201507	LkHa 198	V376 Cas	20.0	38.4	9.6

Table 3: *Photometry of additional sources which were unintentionally observed in maps centred on the main targets of the observers ("original source").*

position (TDT) which is centred on the source and ignored those map positions where the source is located at the border of the camera array. In Table 4 we reviewed the affected sources, and listed the relevant TDT numbers.

Affected sources	TDT numbers
[CCE98] 2- 24, [CCE98] 1- 42	70401408, 70401409, 70401410
[CCE98] 1- 40	70401404, 70401405
[CCE98] 1- 53, [CCE98] 1- 56, V* CU Cha	70401412, 70401415, 70401418

Table 4: *The list of TDT numbers which were combined to extract photometry for a source or for tight group of sources.*

5.3 Other issues

28201104:
Here we extracted photometry assuming a single point source, but it is likely that three far-infrared sources (LkHa 198, LkHa 198-IR, LkHa 198-MM) contribute to the measured flux (Ábrahám et al., 2000).

References

Ábrahám, P., Leinert, C., Burkert, A., Henning, Th., & Lemke, D., 2000, A&A, 354, 965

del Burgo, C., Héraudeau, P., & Ábrahám, P. Exploiting the ISO Data Archive. Infrared Astronomy in the Internet Age, held in Siguenza, Spain 24-27 June, 2002. Edited by C. Gry, S. Peschke, J. Matagne, P. Garcia-Lario, R. Lorente, & A. Salama. Published as ESA Publications Series, ESA SP-511. European Space Agency, 2003, p. 339.

Froebrich, D., Smith, M. D., Hodapp, K.-W., & Eislöffel, J. 2003, MNRAS, 346, 163

Gabriel C., Acosta-Pulido, J., Heinrichsen, I., et al., 1997, in Proc. of the ADASS VI conference (Eds.: G. Hunt, H.E. Payne, ASP Conf.Ser. 125), 108

Juhász, A., Prusti, T., Ábrahám, P., Dullemond, C. P., 2006, astro-ph/0612270

Moór, A., Ábrahám, P., Kiss, Cs., Csizmadia, Sz., 2003, *Far-infrared observations of normal stars measured with ISOPHOT in mini-map mode*, report on Highly Processed Data Products, Version 1.1, available on-line at the ISO Data Centre: *http://pma.iso.vilspa.esa.es:8080/hpdp/technical_reports/technote38.html*

Moór, A., Ábrahám, P., Kiss, Cs., Csizmadia, Sz., 2005, *Catalogue of far-infrared ISOPHOT observations of compact objects in nodding and scan mode*, report on Highly Processed Data Products, available on-line at the ISO Data Centre: *http://ida.esac.esa.int:8080/hpdp/technical_reports/technote31.html*

Appendix: description of the catalogue

The flux densities and their uncertainties for young stellar objects, resulted from the data reduction described in this document, were listed in a photometric catalogue which is included as Highly Processed Data Product. In the following we shall describe the fields of the catalogue.

Column	Field	Unit	Description
(1)	Object name		SIMBAD compatible name or target name as given by the original ISO proposer.
(2)	Object type		Standard SIMBAD code for object type.
(3)	ISO name		Object name given by the ISO observer.
(4)	TDTNUM_ON		The 8-digit TDTNUM of the on-source observation.
(5)	On_ Meas.		Index of the on-source measurement within TDTNUM_ ON.
(6)	AOT		Astronomical Observation Template.
(7)	Observing mode		Observing mode (e.g. mini-map).
(8)	RA(2000)		Right ascension, h:m:s.
(9)	Dec(2000)		Declination, d:m:s.
(10)	Detector		ISOPHOT detector (P1, P2, P3, C100, or C200).
(11)	Wavelength	[micron]	Nominal wavelength of the ISOPHOT filter.
(12)	Aperture	[arcsec]	Aperture for detectors, circular for P1,P2,P3, square for C100 and C200 detectors.
(13)	Epoch		Epoch of the observation.
(14)	TDTNUM_ OFF		The 8-digit TDTNUM of the off-source observation.
(15)	Off_Meas.		Index of the off-source measurement within TDTNUM_OFF.
(16)	Flux density	[Jy]	Flux density of the source. In case of a point source the measured flux is corrected for the size of the point spread function. In case of an extended source it corresponds to the integrated brightness. No colour correction applied.
(17)	Flux uncertainty	[Jy]	Flux uncertainty. No colour correction applied.
(18)	Background	[MJy/sr]	Background surface brightness. No colour correction applied.
(19)	Object size		Indicates if the object is point-like (P) or extended (E).
(20)	Quality		Quality of the observation. R1 – Standard processing according to the scheme described in the report. R2 – Default FCS is used. R3 – Fitting smooth baseline to the data points failed, drift correction (partly/completely) omitted. R4 – Observation was carried out at the very beginning or at the very end of orbit. Reduced photometric reliability at orbital phase lesser than 0.2. R5 – The first measurement in a sparse map sequence generally less reliable due to the non-stabilized signal.

Table 5: Description of the catalogue